Available at
www.ElsevierMathematics.com
POWERED BY SCIENCE DIRECT®

ELSEVIER Computers and Mathematics with Applications 46 (2003) 1711–1724

An International Journal
computers & mathematics
with applications

www.elsevier.com/locate/camwa

# Precise Calibration Method of Pseudolite Positions in Indoor Navigation Systems

CHANGDON KEE, DOOHEE YUN AND HAEYOUNG JUN
School of Mechanical and Aerospace Engineering
Seoul National University
Shillimdong, Kwanak-gu, Seoul, Korea, 151-742

⟨kee⟩⟨aerochol⟩⟨hyjun⟩@snu.ac.kr

*(Received July 2001; revised and accepted May 2002)*

**Abstract**—A pseudolite is a signal generator that transmits a GPS-like signal. Using pseudolites, we developed an indoor navigation system. An indoor navigation system has several positioning error sources, such as time-tag error, multipath error, near/far problem, and pseudolite position error. Among them, we can remove the pseudolite position error by precise calibration because pseudolites are fixed. Otherwise, there would be bias-type positioning errors in indoor navigation solutions. Therefore, how exactly the pseudolite positions are calibrated determines the limit of the indoor navigation system's performance. With this motivation, we made efforts to develop a precise calibration method of pseudolite positions in an indoor navigation system. This paper proposes a practical and accurate calibration method, which uses only pseudolite signals. Simulation results showed that we can calibrate all the pseudolite positions within two or three centimetres by this method. 

**Keywords**—Pseudolite, Indoor navigation system, Pseudolite position calibration, GPS.

## NOMENCLATURE

### Indoor Navigation System Using Pseudolites

| | |
|---|---|
| $\mathbf{R}^i$ | position vector of the $i^{th}$ pseudolite's antenna (3 by 1) |
| $\bar{\mathbf{R}}^i$ | guessed position vector of the $i^{th}$ pseudolite's antenna (3 by 1) |
| $\delta\mathbf{R}^i$ | perturbation of position vector of the $i^{th}$ pseudolite's antenna (3 by 1) |
| $\mathbf{R}_r$ | position vector of the reference station receiver's antenna (3 by 1) |
| $\mathbf{R}_u$ | position vector of the user receiver's antenna (3 by 1) |
| $b^i$ | clock bias of the $i^{th}$ pseudolite (metre) |
| $B_r$ | clock bias of the reference station receiver (metre) |
| $B_u$ | clock bias of the user receiver (metre) |

This research was supported by a grant from the International Joint Research of the Ministry of Information and Communication, Korea, and by a grant from the BK-21 program for Mechanical and Aerospace Engineering Research at Seoul National University. We would like to thank them for their support.

0898-1221/03/$ - see front matter 
doi: 10.1016/S0898-1221(03)00397-3

Typeset by $\mathcal{AMS}$-TEX

$\phi_r^i$ carrier phase of the $i^{th}$ pseudolite, which is measured by reference station's receiver (metre)

$\phi_u^i$ carrier phase of the $i^{th}$ pseudolite, which is measured at user's receiver (metre)

$N$ integer cycle ambiguity

$\hat{\mathbf{e}}$ unit line of sight vector (1 by 3)

$\lambda$ GPS L1 carrier-wave length

$\epsilon_\phi$ carrier phase measurement noise

### Precise Pseudolite Position Calibration Procedure

$\mathbf{R_c}$ position vector of calibration point (3 by 1)

$\phi_c^i$ carrier phase of the $i^{th}$ pseudolite, which is measured at calibration point (metre)

$\sigma^2$ covariance of the carrier-phase measurement noise

$m$ number of pseudolites

$k$ number of calibration points

## INTRODUCTION

A pseudolite is a signal generator, which transmits a GPS-like signal. It can therefore be used as another GPS signal source. If we use signals from pseudolites and GPS satellites together, the system has many advantages, such as geometry augmentation, integrity improvement, and fast cycle ambiguity resolution. However, we need to solve many problems to use pseudolites successfully.

Recently, many research results on pseudolite technology have been reported. In the air navigation applications, Cohen and Cobb produced the Integrity Beacon Landing System (IBLS) for flight inspection in 1994 [1]. They used the IBLS to resolve carrier-phase cycle ambiguity. In the land-based applications, Elkaim and O'Connor controlled a robotic tractor using carrier-phase differential GPS (CDGPS) with the assistance of pseudolites in 1995 [2]. Stone developed a precise positioning system using GPS satellites and pseudolites for open pit mining in 1999 [3]. In this research, he used carrier-phase measurements from both pseudolites and GPS satellites to calculate the user's position.

In indoor applications, Zimmerman conducted a space-vehicle rendezvous in 1996 [4], and Teague studied flexible structure estimation and control using pseudolite signals in 1997 [5]. Olsen and Park made 3D formation flights, using differential carrier-phase GPS sensors indoors [6]. Among the many applications, we were interested in indoor navigation systems using pseudolites. This indoor navigation system has several positioning error sources, such as time-tag error, multipath error, the near/far problem, and pseudolite position error [7]. The first error comes from nonsynchronized receiver sampling time and we can solve it by use of pseudolite navigation message frame. This requires firmware modification of GPS receiver. The second error is generated by reflective objects in indoor navigation environment, such as desks, chairs, cabinets, computers, walls, ceiling, and floor. To minimize the multipath error, we used handmade helical antennae and controlled gain patterns. The third error is a general problem of code division multiple access (CDMA) communication systems. We used a 10% RTCM pulsing scheme to solve this problem. The last error comes from inaccurate calibration of pseudolite positions. We can solve this problem if we calibrate pseudolite positions precisely.

The goal of this paper is to develop a practical and accurate pseudolite calibration method. To be practical, we had to avoid using additional tools, such as laser devices or tape measures. In other words, we used only pseudolite signals measured at calibration points. To be accurate, we needed to optimize calibration points for a given pseudolite constellation to minimize calibration errors. With that in mind, we developed a procedure for calibrating pseudolite positions. As this method uses carrier-phase measurements, we can calibrate the exact phase centre of pseudolite antennae. If we used other survey tools, it would be impossible to calibrate the position of the exact phase centre of pseudolite antennae.

We divided this paper into three sections: theory, simulation, and conclusions. In the theory section, we introduce an indoor navigation system using pseudolites and precise pseudolite posi-

tion calibration procedure. In the simulation section, we summarized simulation results for this calibration procedure using some indoor navigation system configuration and analyzed calibration errors for several cases. In the last section, we gave our conclusions.

# THEORY

## Indoor Navigation System Using Pseudolites

The indoor navigation system is composed of pseudolites, a reference station, and a user, as shown in Figure 1. An indoor navigation system differs from an outdoor navigation system, which uses GPS satellite signals in some parts, as mentioned in the Introduction. Figure 2 shows the handmade helical antennae for pseudolite signal transmission. We chose a helical antennae because we can easily control its gain pattern by varying the number of coil turns [8]. Indoor navigation equations are nonlinear. This is because the distance between pseudolite and receiver antenna is too short for the waveform to be considered plane. This makes us use an iterative method to calculate the user's position. Pseudolite is fixed at one point, while GPS satellites are in the orbital motion at high speed, so that we can remove pseudolite position errors permanently once we precisely calibrate its positions.

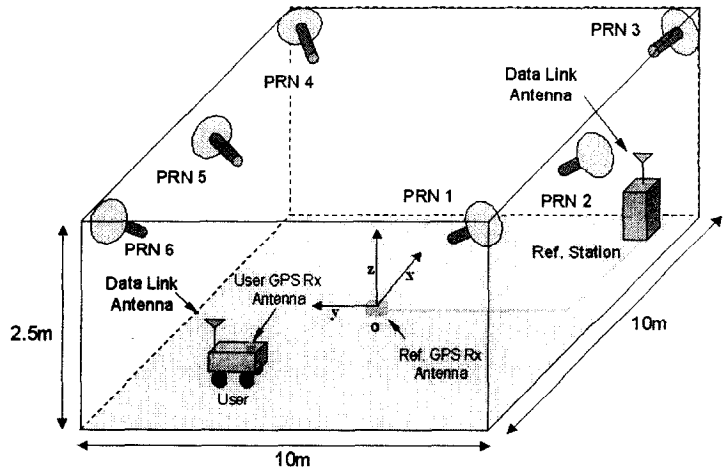


Figure 1. Overview of indoor navigation system using pseudolites.

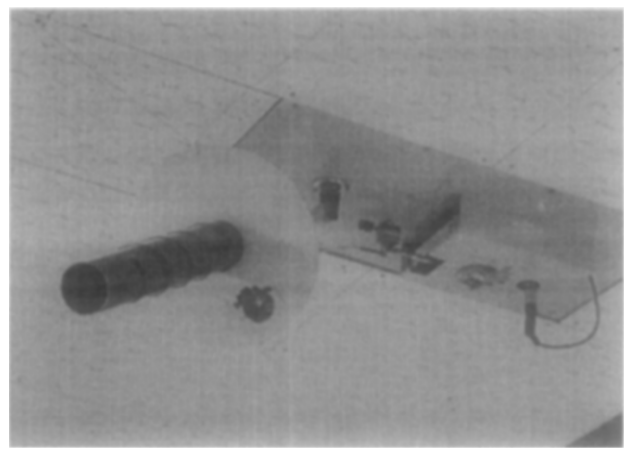

Figure 2. Pseudolite and helical antenna for signal transmission.

Figure 3 shows indoor navigation carrier-phase measurements $\phi_u^i, \phi_u^j, \phi_r^i, \phi_r^j$. Superscripts '$i$' and '$j$' mean the $i^{\text{th}}$ and $j^{\text{th}}$ pseudolite, respectively. Subscripts '$u$' and '$r$' mean user and reference station, respectively. Pseudolite carrier-phase measurements are modelled by equation (1):

$$\begin{aligned}
\phi_u^i &= \left|\mathbf{R^i} - \mathbf{R_u}\right| + B_u - b^i + \lambda \cdot N_u^i + \varepsilon_{\phi_u^i}, \\
\phi_u^j &= \left|\mathbf{R^j} - \mathbf{R_u}\right| + B_u - b^j + \lambda \cdot N_u^j + \varepsilon_{\phi_u^j}, \\
\phi_r^i &= \left|\mathbf{R^i} - \mathbf{R_r}\right| + B_r - b^i + \lambda \cdot N_r^i + \varepsilon_{\phi_r^i}, \\
\phi_r^j &= \left|\mathbf{R^j} - \mathbf{R_r}\right| + B_r - b^j + \lambda \cdot N_r^j + \varepsilon_{\phi_r^j}.
\end{aligned} \tag{1}$$

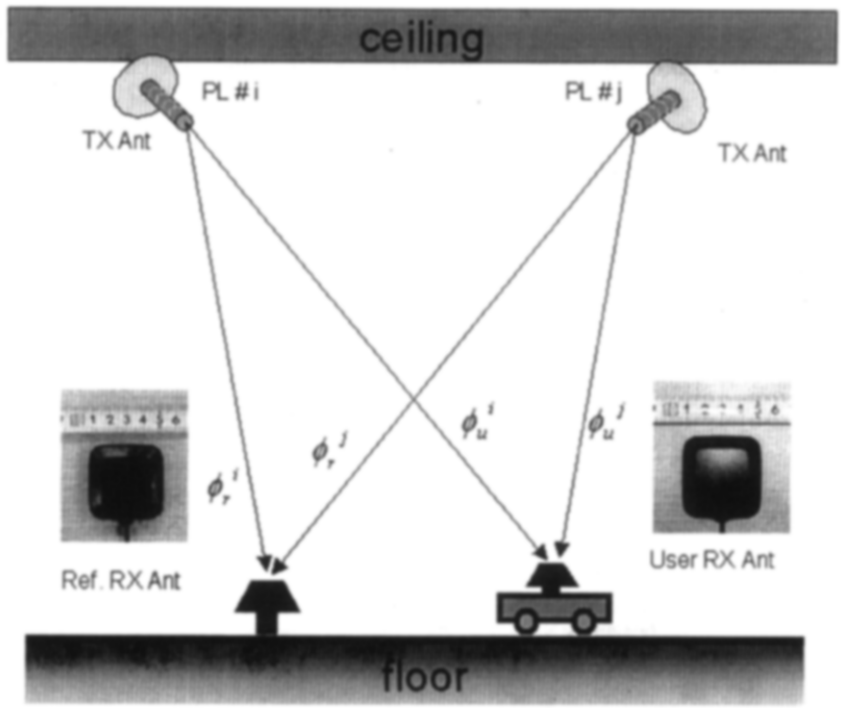


Figure 3. Indoor navigation carrier-phase measurements and receiver antenna.

As there is no atmospheric effect in the indoor environment, there are no ionospheric and tropospheric time delay terms in equation (1). In addition, cycle ambiguities $(N_u^i, N_u^j, N_r^i, N_r^j)$ are constant integer biases unless cycle slip occurs. Equation (2) defines single-differenced carrier-phase measurement between the $i^{\text{th}}$ and $j^{\text{th}}$ pseudolites:

$$^i\Delta^j\phi_u \equiv \phi_u^i - \phi_u^j, \qquad ^i\Delta^j\phi_r \equiv \phi_r^i - \phi_r^j. \tag{2}$$

If we apply another difference operation for single-differenced carrier-phase measurements as equation (3), we can obtain double-differenced carrier-phase measurement and linearize it about guessed pseudolite positions as equation (4):

$$^i\nabla^j{}_u\Delta_r\phi \equiv {}^i\Delta^j\phi_u - {}^i\Delta^j\phi_r, \tag{3}$$

$$^i\nabla^j{}_u\Delta_r\phi = \left|\mathbf{R^i} - \mathbf{R_u}\right| - \left|\mathbf{R^i} - \mathbf{R_r}\right| - \left|\mathbf{R^j} - \mathbf{R_u}\right| + \left|\mathbf{R^j} - \mathbf{R_r}\right| + \lambda \cdot {}^i\nabla^j{}_u\Delta_r N + \varepsilon_{{}^i\nabla^j{}_u\Delta_r\phi}, \tag{4}$$

where $^i\nabla^j{}_u\Delta_r N \equiv N_u^i - N_u^j - (N_r^i - N_r^j)$, $\varepsilon_{{}^i\nabla^j{}_u\Delta_r\phi} \equiv \varepsilon_{\phi_u^i} - \varepsilon_{\phi_u^j} - (\varepsilon_{\phi_r^i} - \varepsilon_{\phi_r^j})$.

By using a double difference operation, clock biases of pseudolite and receiver are removed and the number of independent measurements decreases by one. In other words, we can obtain $m-1$ independent double-differenced carrier phase measurements for $m$ pseudolites.

## Precise Pseudolite Position Calibration Procedure

We developed a precise pseudolite position calibration procedure for an indoor navigation system as shown in Figure 4. This procedure contains two subproblems. One is to optimize calibration points[1] set for estimated pseudolite positions. The other is to calculate pseudolite positions using double-differenced carrier-phase measurements collected at the optimized calibration points set. We can summarize the whole procedure as follows. At first, we should estimate all the pseudolite positions after pseudolites are installed. It is possible to estimate all the pseudolite positions within one metre by eye. We then should decide how many calibration points are used and optimize calibration points set for the estimated pseudolite positions. After we collect carrier-phase measurements at all the optimized calibration points, we calculate pseudolite positions and check convergence. If all the pseudolite positions converge satisfactorily, we can finish this procedure. Otherwise, we should update the initial estimate of pseudolite positions and then repeat this procedure until convergence. Generally, two or three iterations are sufficient. This is a "*precise calibration method of pseudolite positions in indoor navigation system*". We will give detailed explanations of these two subproblems in the following sections.

We believe this method is practical and accurate because no additional tools such as laser devices or tape measures are required and calibrated pseudolite positions are not physical centres of transmission antennas, but their phase centres. However, this method also has a problem. That is how we can ensure that the actual phase centre of the calibration antenna be physically placed precisely at the calibration points. We solved this problem by engineering sense. Figure 5 shows a flat patch antenna, which is a calibration receiver antenna, and 'X' marks on the floor, which represent calibration points. The size of patch antenna is small and its physical phase-centre information can be obtained from the manufacturer. So we think it is possible to place the actual phase centre of the receiver's antenna at the calibration points within reasonable small errors.

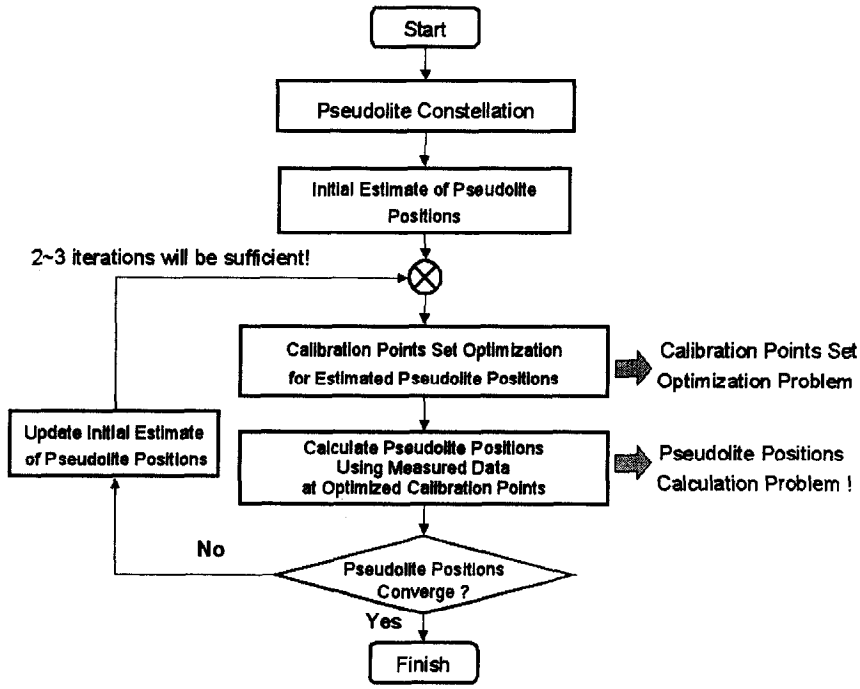


Figure 4. Precise calibration procedure of pseudolite positions for an indoor navigation system.

[1]The points set on the floor where the user receiver's antenna are placed and carrier-phase measurements are collected to calibrate pseudolite positions.

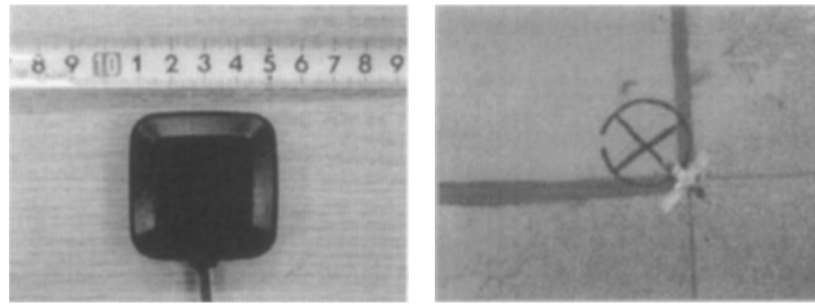

Figure 5. Patch antenna and 'X' marks on the floor that represent calibration points.

## Subproblem: Optimization of Calibration Points Set for the Estimated Pseudolite Positions

To solve this subproblem, we used the following assumptions.

1. Reference station antenna is fixed and its position is known exactly.
2. Calibration points should be within valid indoor navigation area.
3. Cycle ambiguities can be resolved directly by initial data logging condition (Figure 6).
4. There is no cycle slip during collection of carrier-phase measurements.
5. Carrier-phase measurement noise is a zero-mean white Gaussian random variable.

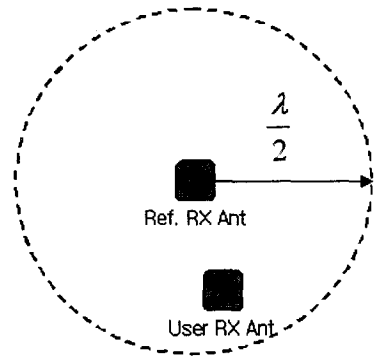


Figure 6. User receiver's antenna position that makes all the double differenced cycle ambiguities zero.

Assumption 2 means this is a constrained optimization problem. Naturally, calibration points are restricted to valid indoor navigation area. If we place the user receiver's antenna within half a wavelength from the reference station receiver's antenna as in Figure 6, baseline length between two antennas is less than half a wavelength. So the maximum magnitude of the double differenced carrier phase becomes less than one wavelength. If we start data logging with this condition, all the cycle ambiguities become zero. This is Assumption 3. And then we should move the user receiver's antenna to every calibration point very carefully lest any cycle slip should occur. This is Assumption 4. Due to these two assumptions, we can remove all the cycle ambiguities from double differenced carrier-phase measurements and optimization performance index. With all the above assumptions, we define this subproblem as the following. *"To determine optimal calibration points set, which minimizes pseudolite position calibration errors for estimated pseudolite positions."*

As we calculate pseudolite positions by use of weighted least-square estimation, it is natural to take error covariance as the optimization performance index. However, it is difficult to calculate the error covariance matrix because the original measurement equations are nonlinear. So, we linearized equation (4) about guessed pseudolite positions and applied Assumption 4. We then

obtained equation (5):

$$
\begin{aligned}
{}^{i}\nabla^{j}{}_{u}\Delta_{r}\phi \cong & \left|\bar{\mathbf{R}}^{\mathbf{i}}-\mathbf{R}_{\mathbf{u}}\right|-\left|\bar{\mathbf{R}}^{\mathbf{i}}-\mathbf{R}_{\mathbf{r}}\right|-\left|\bar{\mathbf{R}}^{\mathbf{j}}-\mathbf{R}_{\mathbf{u}}\right|+\left|\bar{\mathbf{R}}^{\mathbf{j}}-\mathbf{R}_{\mathbf{r}}\right|+\left(\hat{\mathbf{e}}_{\mathbf{u}}^{\mathbf{i}}\big|_{\bar{\mathbf{R}}^{\mathbf{i}}}-\hat{\mathbf{e}}_{\mathbf{r}}^{\mathbf{i}}\big|_{\bar{\mathbf{R}}^{\mathbf{i}}}\right)\cdot\delta\mathbf{R}^{\mathbf{i}} \\
& -\left(\hat{\mathbf{e}}_{\mathbf{u}}^{\mathbf{j}}\big|_{\bar{\mathbf{R}}^{\mathbf{j}}}-\hat{\mathbf{e}}_{\mathbf{r}}^{\mathbf{j}}\big|_{\bar{\mathbf{R}}^{\mathbf{j}}}\right)\cdot\delta\mathbf{R}^{\mathbf{j}}+\varepsilon_{i\nabla^{j}{}_{u}\Delta_{r}\phi},
\end{aligned}
\tag{5}
$$

where

$$
\begin{aligned}
\delta\mathbf{R}^{\mathbf{i}} &= \mathbf{R}^{\mathbf{i}}-\bar{\mathbf{R}}^{\mathbf{i}}, & \delta\mathbf{R}^{\mathbf{j}} &= \mathbf{R}^{\mathbf{j}}-\bar{\mathbf{R}}^{\mathbf{j}}, \\
\mathbf{e}_{\mathbf{u}}^{\mathbf{i}}\big|_{\bar{\mathbf{R}}^{\mathbf{i}}} &\equiv \frac{\left|\mathbf{R}^{\mathbf{i}}-\mathbf{R}_{\mathbf{u}}\right|}{\left|\bar{\mathbf{R}}^{\mathbf{i}}-\mathbf{R}_{\mathbf{u}}\right|}, & \hat{\mathbf{e}}_{\mathbf{r}}^{\mathbf{i}}\big|_{\bar{\mathbf{R}}^{\mathbf{i}}} &\equiv \frac{\left|\mathbf{R}^{\mathbf{i}}-\mathbf{R}_{\mathbf{r}}\right|}{\left|\bar{\mathbf{R}}^{\mathbf{i}}-\mathbf{R}_{\mathbf{r}}\right|}.
\end{aligned}
$$

If we rearrange equation (5) and replace the user's position with a calibration point, we can obtain equation (6):

$$
\begin{aligned}
\left(\hat{\mathbf{e}}_{\mathbf{r}}^{\mathbf{i}}\big|_{\bar{\mathbf{R}}^{\mathbf{i}}}-\hat{\mathbf{e}}_{\mathbf{c}}^{\mathbf{i}}\big|_{\bar{\mathbf{R}}^{\mathbf{i}}}\right)\cdot\mathbf{R}^{\mathbf{i}}-\left(\hat{\mathbf{e}}_{\mathbf{r}}^{\mathbf{j}}\big|_{\bar{\mathbf{R}}^{\mathbf{j}}}-\hat{\mathbf{e}}_{\mathbf{c}}^{\mathbf{j}}\big|_{\bar{\mathbf{R}}^{\mathbf{j}}}\right)\cdot\mathbf{R}^{\mathbf{j}} &= \left(\hat{\mathbf{e}}_{\mathbf{r}}^{\mathbf{i}}\big|_{\bar{\mathbf{R}}^{\mathbf{i}}}-\hat{\mathbf{e}}_{\mathbf{c}}^{\mathbf{i}}\big|_{\bar{\mathbf{R}}^{\mathbf{i}}}\right)\cdot\bar{\mathbf{R}}^{\mathbf{i}}-\left(\hat{\mathbf{e}}_{\mathbf{r}}^{\mathbf{j}}\big|_{\bar{\mathbf{R}}^{\mathbf{j}}}-\hat{\mathbf{e}}_{\mathbf{c}}^{\mathbf{j}}\big|_{\bar{\mathbf{R}}^{\mathbf{j}}}\right)\cdot\bar{\mathbf{R}}^{\mathbf{j}} \\
&+\left|\bar{\mathbf{R}}^{\mathbf{i}}-\mathbf{R}_{\mathbf{c}}\right|-\left|\bar{\mathbf{R}}^{\mathbf{i}}-\mathbf{R}_{\mathbf{r}}\right|-\left|\bar{\mathbf{R}}^{\mathbf{j}}-\mathbf{R}_{\mathbf{c}}\right|+\left|\bar{\mathbf{R}}^{\mathbf{j}}-\mathbf{R}_{\mathbf{r}}\right|-{}^{i}\nabla^{j}{}_{c}\Delta_{r}\phi+\varepsilon_{i\nabla^{j}{}_{c}\Delta_{r}\phi}.
\end{aligned}
\tag{6}
$$

There are $m-1$ independent equations for the $k^{\text{th}}$ calibration point and we can express them in one matrix equation as follows:

$$
\begin{bmatrix}
+{}_{\mathrm{r}}\Delta_{\mathrm{c}}\hat{\mathbf{e}}^{1}\big|_{\bar{\mathbf{R}}^{1}} & -{}_{\mathrm{r}}\Delta_{\mathrm{c}}\hat{\mathbf{e}}^{2}\big|_{\bar{\mathbf{R}}^{2}} & \mathbf{O}_{1\times3} & \cdots & \mathbf{O}_{1\times3} & \mathbf{O}_{1\times3} \\
\mathbf{O}_{1\times3} & +{}_{\mathrm{r}}\Delta_{\mathrm{c}}\hat{\mathbf{e}}^{2}\big|_{\bar{\mathbf{R}}^{2}} & -{}_{\mathrm{r}}\Delta_{\mathrm{c}}\hat{\mathbf{e}}^{3}\big|_{\bar{\mathbf{R}}^{3}} & \cdots & \mathbf{O}_{1\times3} & \mathbf{O}_{1\times3} \\
\mathbf{O}_{1\times3} & \mathbf{O}_{1\times3} & +{}_{\mathrm{r}}\Delta_{\mathrm{c}}\hat{\mathbf{e}}^{3}\big|_{\bar{\mathbf{R}}^{3}} & \ddots & \mathbf{O}_{1\times3} & \mathbf{O}_{1\times3} \\
\vdots & \vdots & \vdots & \ddots & \vdots & \vdots \\
\mathbf{O}_{1\times3} & \mathbf{O}_{1\times3} & \mathbf{O}_{1\times3} & \cdots & -{}_{\mathrm{r}}\Delta_{\mathrm{c}}\hat{\mathbf{e}}^{m-1}\big|_{\bar{\mathbf{R}}^{m-1}} & \mathbf{O}_{1\times3} \\
\mathbf{O}_{1\times3} & \mathbf{O}_{1\times3} & \mathbf{O}_{1\times3} & \cdots & +{}_{\mathrm{r}}\Delta_{\mathrm{c}}\hat{\mathbf{e}}^{m-1}\big|_{\bar{\mathbf{R}}^{m-1}} & -{}_{\mathrm{r}}\Delta_{\mathrm{c}}\hat{\mathbf{e}}^{m}\big|_{\bar{\mathbf{R}}^{m}}
\end{bmatrix}
$$

$$
\cdot\begin{Bmatrix}\mathbf{R}^{1}\\ \mathbf{R}^{2}\\ \vdots\\ \mathbf{R}^{\mathbf{m-1}}\\ \mathbf{R}^{\mathbf{m}}\end{Bmatrix}=\begin{Bmatrix}z_{12}\\ z_{23}\\ \vdots\\ z_{m-2m-1}\\ z_{m-1m}\end{Bmatrix}+\begin{Bmatrix}\varepsilon_{1\nabla^{2}{}_{c}\Delta_{r}\phi}\\ \varepsilon_{2\nabla^{3}{}_{c}\Delta_{r}\phi}\\ \vdots\\ \varepsilon_{m-2\nabla^{m-1}{}_{c}\Delta_{r}\phi}\\ \varepsilon_{m-1\nabla^{m}{}_{c}\Delta_{r}\phi}\end{Bmatrix}
\tag{7}
$$

$$
\Rightarrow \mathbf{h}_{\mathbf{l}}(\mathbf{R}_{\mathbf{c}})\cdot\mathbf{x}_{\mathbf{p}}=\mathbf{z}_{\mathbf{l}}(\mathbf{R}_{\mathbf{c}})+\mathbf{v}_{\nabla\Delta\phi},
$$

where

$$
\begin{aligned}
{}_{\mathrm{r}}\Delta_{\mathrm{c}}\,\hat{\mathbf{e}}^{\mathbf{i}}\big|_{\bar{\mathbf{R}}^{\mathbf{i}}} &\equiv \hat{\mathbf{e}}_{\mathbf{r}}^{\mathbf{i}}\big|_{\bar{\mathbf{R}}^{\mathbf{i}}}-\hat{\mathbf{e}}_{\mathbf{c}}^{\mathbf{i}}\big|_{\bar{\mathbf{R}}^{\mathbf{i}}}, \\
\mathbf{x}_{\mathbf{p}}^{\top} &= \left\{\mathbf{R}^{\mathbf{1}^{\top}}\quad\mathbf{R}^{\mathbf{2}^{\top}}\quad\cdots\quad\mathbf{R}^{\mathbf{m}^{\top}}\right\}, \\
\mathbf{z}_{\mathbf{l}}(\mathbf{R}_{\mathbf{c}}) &= \left\{z_{12}\quad z_{23}\quad\cdots\quad z_{m-1m}\right\}^{\top}, \\
z_{ij} &= {}_{\mathrm{r}}\Delta_{\mathrm{c}}\hat{\mathbf{e}}^{\mathbf{i}}\big|_{\bar{\mathbf{R}}^{\mathbf{i}}}\cdot\bar{\mathbf{R}}^{\mathbf{i}}-{}_{\mathrm{r}}\Delta_{\mathrm{c}}\hat{\mathbf{e}}^{\mathbf{j}}\big|_{\bar{\mathbf{R}}^{\mathbf{j}}}\cdot\bar{\mathbf{R}}^{\mathbf{j}} \\
&\quad+\left|\bar{\mathbf{R}}^{\mathbf{i}}-\mathbf{R}_{\mathbf{c}}\right|-\left|\bar{\mathbf{R}}^{\mathbf{i}}-\mathbf{R}_{\mathbf{r}}\right|-\left|\bar{\mathbf{R}}^{\mathbf{j}}-\mathbf{R}_{\mathbf{c}}\right|+\left|\bar{\mathbf{R}}^{\mathbf{j}}-\mathbf{R}_{\mathbf{r}}\right|-{}^{i}\nabla^{j}{}_{c}\Delta_{r}\phi+\varepsilon_{i\nabla^{j}{}_{c}\Delta_{r}\phi}, \\
\mathbf{v}_{\nabla\Delta_{\phi}} &= \left\{\varepsilon_{1\nabla2\,{}_{c}\Delta_{r}\phi}\quad\varepsilon_{2\nabla^{3}{}_{c}\Delta_{r}\phi}\quad\cdots\quad\varepsilon_{m-1\nabla^{m}{}_{c}\Delta_{r}\phi}\right\}^{\top}.
\end{aligned}
$$

Generally, multiple calibration points are required to calibrate pseudolite positions. So, we need a multiepoch version of equation (7) as follows:

$$
\begin{bmatrix}\mathbf{h}_{\mathbf{l}}(\mathbf{R}_{\mathbf{c}}(1))\\ \mathbf{h}_{\mathbf{l}}(\mathbf{R}_{\mathbf{c}}(2))\\ \mathbf{h}_{\mathbf{l}}(\mathbf{R}_{\mathbf{c}}(3))\\ \vdots\\ \mathbf{h}_{\mathbf{l}}(\mathbf{R}_{\mathbf{c}}(\mathbf{k}))\end{bmatrix}\cdot\begin{Bmatrix}\mathbf{R}^{1}\\ \mathbf{R}^{2}\\ \vdots\\ \mathbf{R}^{\mathbf{m}}\end{Bmatrix}=\begin{Bmatrix}\mathbf{z}_{\mathbf{l}}(\mathbf{R}_{\mathbf{c}}(1))\\ \mathbf{z}_{\mathbf{l}}(\mathbf{R}_{\mathbf{c}}(2))\\ \mathbf{z}_{\mathbf{l}}(\mathbf{R}_{\mathbf{c}}(3))\\ \vdots\\ \mathbf{z}_{\mathbf{l}}(\mathbf{R}_{\mathbf{c}}(\mathbf{k}))\end{Bmatrix}+\begin{Bmatrix}\mathbf{v}_{\nabla\Delta\phi}(1)\\ \mathbf{v}_{\nabla\Delta\phi}(2)\\ \mathbf{v}_{\nabla\Delta\phi}(3)\\ \vdots\\ \mathbf{v}_{\nabla\Delta\phi}(\mathbf{k})\end{Bmatrix}\Leftrightarrow\mathbf{H}_{\mathbf{l}}(\mathbf{x}_{\mathbf{c}})\cdot\mathbf{x}_{\mathbf{p}}=\mathbf{Z}_{\mathbf{l}}(\mathbf{x}_{\mathbf{c}})+\mathbf{V},
\tag{8}
$$

where

$$\mathbf{x}_c^\top = \{\mathbf{R}_c^\top(1) \quad \mathbf{R}_c^\top(2) \quad \cdots \quad \mathbf{R}_c^\top(k)\},$$
$$\mathbf{V}^\top = \{\mathbf{v}_{\nabla\Delta\phi}^\top(1) \quad \mathbf{v}_{\nabla\Delta\phi}^\top(2) \quad \mathbf{v}_{\nabla\Delta\phi}^\top(3) \quad \cdots \quad \mathbf{v}_{\nabla g\Delta\phi}^\top(k)\}.$$

Let $\hat{\mathbf{x}}_\mathbf{p}$ be an estimated pseudolite position. Then weighted square error (WSE) is

$$\text{WSE} = (\mathbf{Z}_\mathbf{l}(\mathbf{x_c}) - \mathbf{H}_\mathbf{l}(\mathbf{x_c}) \cdot \hat{\mathbf{x}}_\mathbf{p})^\top \cdot \text{cov}[\mathbf{V}]^{-1} \cdot (\mathbf{Z}_\mathbf{l}(\mathbf{x_c}) - \mathbf{H}_\mathbf{l}(\mathbf{x_c}) \cdot \hat{\mathbf{x}}_\mathbf{p}). \tag{9}$$

For $\hat{x}_p$ to become a weighted least-square estimation, equation (10) should be satisfied as a necessary condition:

$$\frac{1}{2}\frac{\partial \text{WSE}}{\partial \hat{\mathbf{x}}_\mathbf{p}} = -\mathbf{H}_\mathbf{l}(\mathbf{x_c})^\top \cdot \text{cov}[\mathbf{V}]^{-1} \cdot (\mathbf{Z}_\mathbf{l}(\mathbf{x_c}) - \mathbf{H}_\mathbf{l}(\mathbf{x_c}) \cdot \hat{\mathbf{x}}_\mathbf{p}) \equiv 0. \tag{10}$$

From equation (10),

$$\hat{\mathbf{x}}_\mathbf{p} = \left(\mathbf{H}_\mathbf{l}(\mathbf{x_c})^\top \cdot \text{cov}[\mathbf{V}]^{-1} \cdot \mathbf{H}_\mathbf{l}(\mathbf{x_c})\right)^{-1} \mathbf{H}_\mathbf{l}(\mathbf{x_c})^\top \cdot \text{cov}[\mathbf{V}]^{-1} \cdot \mathbf{Z}_\mathbf{l}(\mathbf{x_c}). \tag{11}$$

To calibrate pseudolite positions precisely, we should minimize covariance of $\hat{\mathbf{x}}_\mathbf{p}$. Equation (12) shows its covariance:

$$\mathbf{cov}[\hat{\mathbf{x}}_\mathbf{p}] = E[\hat{\mathbf{x}}_\mathbf{p}\hat{\mathbf{x}}_\mathbf{p}^\top] = \left(\mathbf{H}_\mathbf{l}(\mathbf{x_c})^\top \mathbf{cov}[\mathbf{V}]^{-1} \mathbf{H}_\mathbf{l}(\top \mathbf{x_c})\right)^{-1}. \tag{12}$$

Equation (12) shows that pseudolite position errors depend on $\mathbf{H_l}(\mathbf{x_c})$ and $\mathbf{cov}[\mathbf{V}]$. $\mathbf{H_l}(\mathbf{x_c})$ is determined by pseudolites and calibration point sets. As pseudolites are fixed, we should optimize calibration points set to minimize $\mathbf{cov}[\hat{\mathbf{x}}_\mathbf{p}]$. $\mathbf{cov}[\mathbf{V}]$ is determined by carrier-phase measurement noise ($\sigma$) and double-difference operation matrix ($\mathbf{A}$) as

$$\mathbf{cov}[\mathbf{V}] = \mathbf{2AA}^\top\sigma^2, \tag{13}$$

where

$$\mathbf{A} = \begin{bmatrix} \mathbf{a} & & \\ & \mathbf{a} & \\ & & \ddots \\ & & \mathbf{a} \end{bmatrix}_{k(m-1)\times km}, \qquad \mathbf{a} = \begin{bmatrix} +1 & -1 & 0 & 0 & 0 & 0 \\ 0 & +1 & -1 & 0 & 0 & 0 \\ 0 & 0 & +1 & \ddots & 0 & 0 \\ 0 & 0 & 0 & \ddots & -1 & 0 \\ 0 & 0 & 0 & 0 & +1 & -1 \end{bmatrix}_{(m-1)\times m}.$$

As $\mathbf{cov}[\mathbf{V}]$ is correlated through a double-difference operation, there exist off-diagonal terms. Using (12) and (13), we set the optimization performance index as

$$\text{minimize } J = \text{norm}\left\{\text{diag}\left[\left(\mathbf{H}_\mathbf{l}(\mathbf{x_c})^\top \cdot \left(\mathbf{AA}^\top\right)^{-1} \cdot \mathbf{H}_\mathbf{l}(\mathbf{x_c})\right)^{-1}\right]\right\}, \tag{14}$$

with constraints $x_{\min} \le x_c(i) \le x_{\max}$, $y_{\min} \le y_c(i) \le y_{\max}$, $z_{\min} \le z_c(i) \le z_{\max}$.

In equation (14), $\sigma^2$ does not appear because it is a positive constant so that it does not influence optimization performance index. We used commercial optimization function 'constr.m' in MATLAB© to obtain an optimized calibration points set [9].

### Subproblem: Pseudolite Position Calculation using Measurement

Using double-differenced carrier-phase measurements, which are collected at all the optimized calibration points, we can calculate pseudolite positions as shown in Figure 7. We used the following assumptions in this algorithm.

1. We know exactly all the positions of reference station receiver's antenna and calibration points.
2. We can measure pseudolite positions approximately within one metre by eye.
3. Cycle ambiguities can be resolved directly by initial data logging condition (Figure 6).

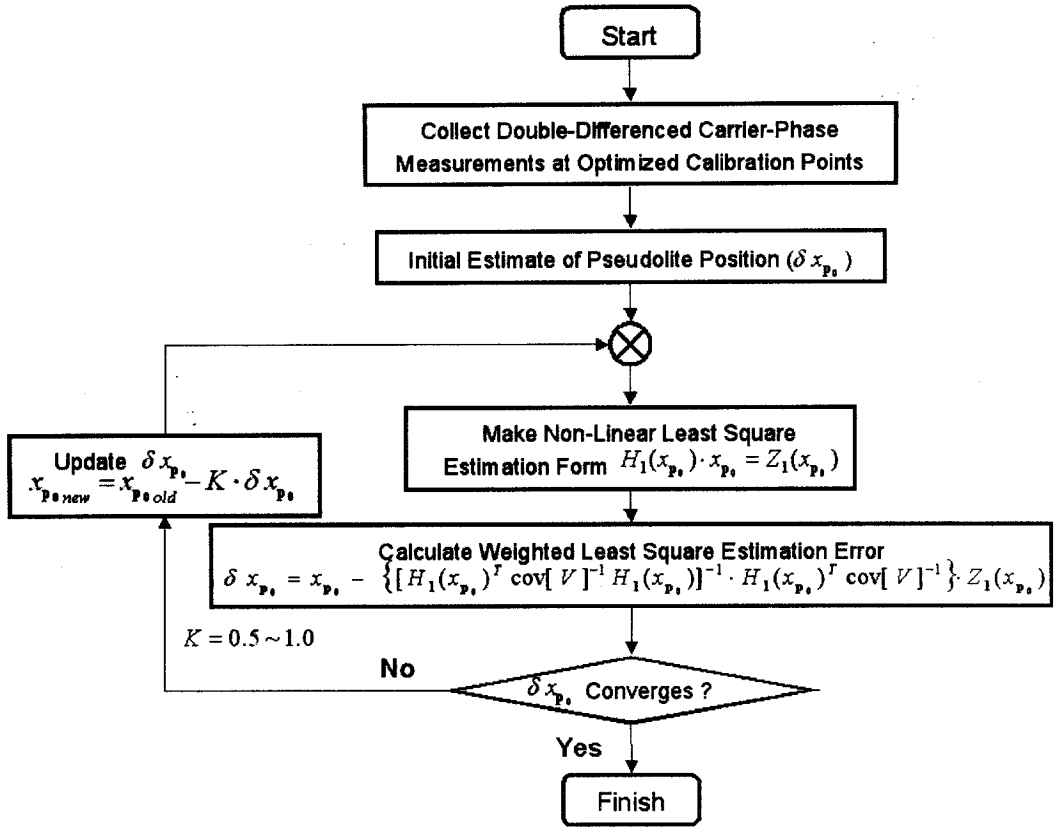


Figure 7. Calculation of pseudolite positions by use of nonlinear weighted least square estimation.

As the observation equation of this subproblem is the same as that of the previous subproblem, we can use equation (8). As this algorithm is a nonlinear iteration, convergence depends on initial conditions. Thus, we need the second assumption. Calculation of pseudolite positions starts with an initial estimate ($\mathbf{x}_{p_0}$) as shown in Figure 7. The next step is to form a nonlinear least square estimation equation and calculate estimation error ($\delta \mathbf{x}_{p_0}$). If pseudolite positions converge sufficiently, this procedure will be finished. Otherwise, we should update the initial estimate by estimation error and repeat this iteration until convergence. This method is a kind of inverse carrier-phase differential GPS (ICDGPS). By the way, to calculate pseudolite positions using equation (8), observation matrix $\mathbf{H}(\mathbf{x}_{p_0})$ should be full rank. That is, the number of independent measurements ($k \times (m-1)$) is greater than the number of unknowns ($3m$). Thus, the following equation should be satisfied:

$$k \geq \frac{3m}{m-1}. \tag{15}$$

Equation (15) is the relationship between the number of pseudolite and minimum number of calibration points. As our indoor navigation system uses six pseudolites as shown in Figure 1. we need at least four calibration points to satisfy equation (15).

## SIMULATION RESULTS

We simulated several pseudolite position calibrations for the indoor navigation set up shown in Figure 1. At first, we optimized calibration points set for two cases—four and six calibration points. To analyze the influence of the reference station receiver's antenna position, we moved the reference station receiver's antenna and calculated traces of optimal calibration points set.

To estimate the effectiveness of our procedure, we compared pseudolite position calibration errors using optimal calibration points set with that using intuitive calibration points set for every case.

## Indoor Navigation System Configuration for Simulation

We summarized indoor navigation system configuration, which was used in all the simulations in Table 1. We set covariance of carrier-phase measurement noise ($\sigma$) as two millimetres and used it for the generation of carrier-phase measurement errors. As calibration points should be in an indoor navigation serviceable area, we set constraints for calibration points as

$$-10.0\,\mathrm{m} \le x_c(i) \le 10.0\,\mathrm{m}, \quad -10.0\,\mathrm{m} \le y_c(i) \le 10.0\,\mathrm{m}, \qquad z_c(i) = 0.0\,\mathrm{m}, \quad i = 1, 2, \ldots, k. \tag{16}$$

Equation (16) means that the indoor navigation area is 20 metres by 20 metres and all the calibration points should be on the floor.

Table 1. Pseudolites and their positions for simulation.

| Pseudolite Number (PRN) | $X$ | $Y$ | $Z$ |
|---|---|---|---|
| 1 | −5.0 m | −5.0 m | +2.5 m |
| 2 | 0.0 m | −5.0 m | +2.0 m |
| 3 | +5.0 m | −5.0 m | +2.5 m |
| 4 | +5.0 m | +5.0 m | +2.5 m |
| 5 | 0.0 m | +5.0 m | +2.0 m |
| 6 | −5.0 m | +5.0 m | +2.5 m |

## Optimal Calibration Points

At first, we optimized calibration points set with reference station receiver's antenna at the origin. And then to estimate the influence of the constraint on optimization, we calculated traces of the optimal points set by extending the constraint from a small area to the whole indoor navigation area, defined by equation (16). Figure 8 is an optimal four calibration points set, which

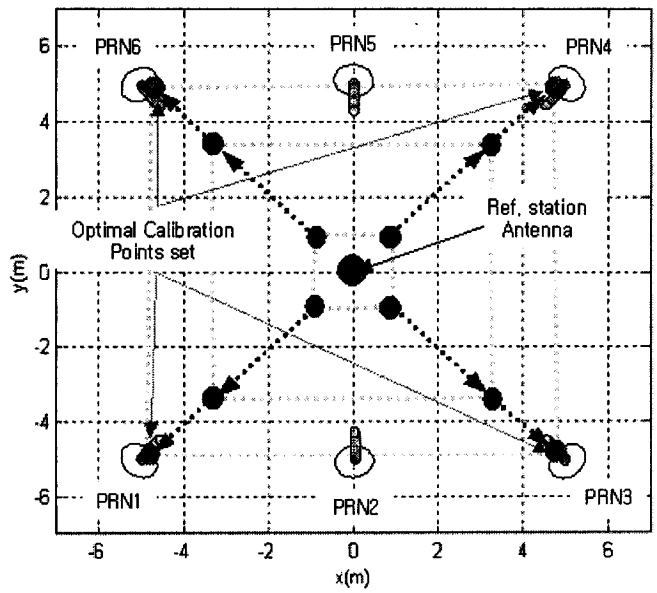


Figure 8. Optimal four calibration points set.

is Case A in Table 2, and Figure 9 shows optimal six calibration points set, which is Case E in Table 2. In both cases, all the optimal calibration points set are perfectly symmetric about the origin. This is reasonable because pseudolite constellation is symmetric about the origin and the reference station receiver's antenna is at the origin.

Table 2. Calibration points set and pseudolite position calibration errors.

| Case | A | B | C |
|---|---|---|---|
| Number of Calibration Points | 4 points | 4 points | 4 points |
| Ref. Station Antenna $(x, y)$ $z = 0$, Unit: Meter | (0.0, 0.0) | (0.0, 0.0) | (0.5, 3.0) |
| Points Set Determination | Optimization | By Intuition (Regular Tetragon[a]) | Optimization |
| Points Set $(x, y)$ $z = 0$ Unit: Meter | (+4.724, +4.892)<br>(+4.724, −4.892)<br>(−4.724, −4.892)<br>(−4.724, +4.892) | (+4.809, +4.809)<br>(+4.809, −4.809)<br>(−4.809, −4.809)<br>(−4.809, +4.809) | (+5.221, +5.859)<br>(+5.401, −4.290)<br>(−2.292, −4.365)<br>(−5.456, +5.467) |
| Pseudolite Position Calibration RMS Error | 0.01621 m | 0.01623 m | 0.01828 m |

| Case | D | E | F |
|---|---|---|---|
| Number of Calibration Points | 4 points | 6 points | 6 points |
| Ref. Station Antenna $(x, y)$ $z = 0$, Unit: Meter | (0.5, 3.0) | (0.0, 0.0) | (0.0, 0.0) |
| Point Set Determination | By Intuition (Regular Tetragon) | Optimization | By Intuition (Regular Hexagon[b]) |
| Points Set $(x, y)$ $z = 0$ Unit: Meter | (+4.809, +4.809)<br>(+4.809, −4.809)<br>(−4.809, −4.809)<br>(−4.809, +4.809) | (+5.129, +5.228)<br>(+5.129, −5.228)<br>(−5.129, −5.228)<br>(−5.129, +5.228)<br>(0.000, +4.884)<br>(0.000, −4.884) | (+5.639, +3.256)<br>(+5.639, −3.256)<br>(−5.639, −3.256)<br>(−5.639, +3.256)<br>(0.000, +6.511)<br>(0.000, −6.511) |
| Pseudolite Position Calibration RMS Error | 0.02146 m | 0.01037 m | 0.01177 m |

[a]We chose the regular tetragon for the radius of circumcircle to be the average distance from the origin of four optimal points in Case A.

[b]We chose the regular hexagon for the radius of circumcircle to be average distance from the origin of six optimal points in Case E.

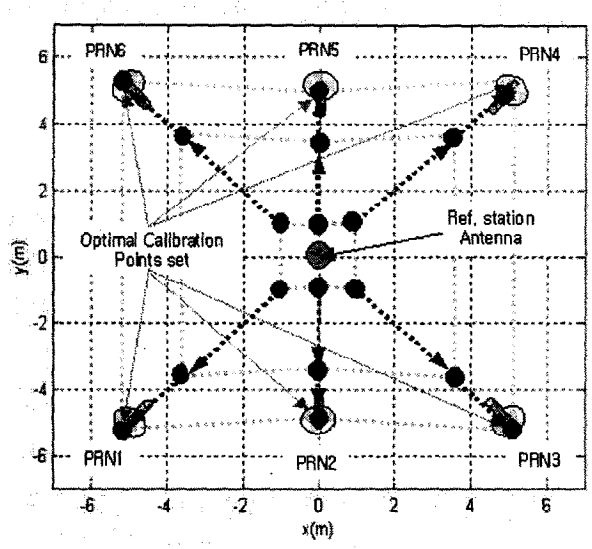


Figure 9. Optimal six calibration points set.

## Influence of Reference Station Receiver's Antenna Position on the Optimization of Calibration Points Set

Error covariance of pseudolite positions is a function of both calibration points set and reference station receiver's antenna position. Therefore, the optimal calibration points set will change if we move the reference station receiver's antenna. To analyze this, we moved the reference station receiver's antenna position from (0.0 m, 0.0 m, 0.0 m) to (0.5 m, 3.0 m, 0.0 m) and optimized calibration points set for four points case. Figure 10 is a trace of the optimal calibration points set. As expected, the optimal calibration points set varied as the reference station receiver's antenna moved. Figure 10 shows that if the reference station receiver's antenna is not at the origin or on the axis, the optimal calibration points set is no longer symmetric. This means that we cannot obtain optimal calibration points set using symmetric intuition, while it was possible when the reference station receiver's antenna is at the origin. Therefore, our procedure is much more useful when the reference station receiver's antenna is not located symmetrically.

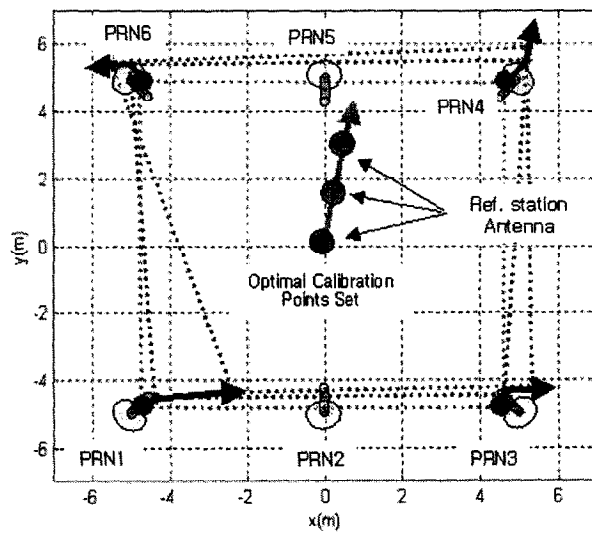


Figure 10. Trace of optimal calibration points set according to the reference station receiver's antenna position.

### Performance Comparison: Optimal Calibration Points Set vs. Intuitive Calibration Points Set

To estimate how much pseudolite position calibration errors can be reduced by use of optimal calibration points set, we simulated pseudolite position calibrations using different four calibration points sets, which are Case A, Case B, Case C, and Case D in Table 2. We executed 1,000 simulations for every case to obtain sufficiently accurate statistical pseudolite position calibration errors. Figure 11 shows results for each case. These simulation results show that an optimal calibration points set is better than an intuitive calibration points set. The improvement from Case D to Case C is greater than from Case B to Case A. This means that optimization of calibration points set is more significant when the reference station receiver's antenna is not located at the origin nor on the axis.

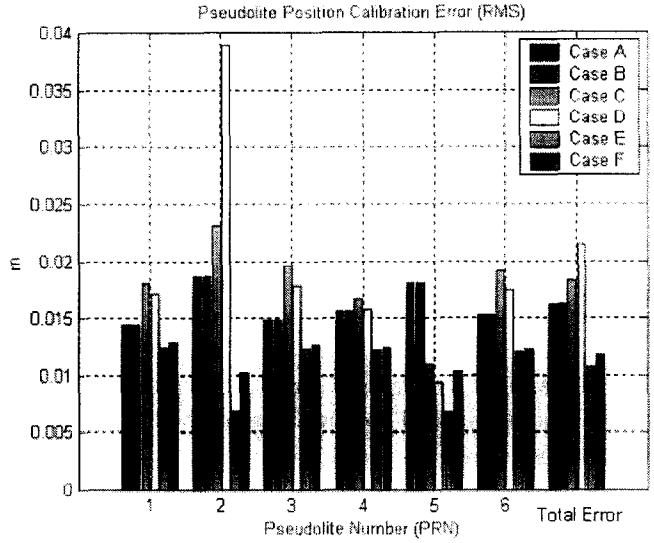


Figure 11. Comparison of pseudolite calibration errors.

### Performance Comparison: Four Calibration Points Set vs. Six Calibration Points Set

To analyze the influence of the number of calibration points on the pseudolite position calibration errors, we compared calibration errors using four calibration points sets, which are Case A, Case B, Case E, and Case F in Table 2. We summarize the results in Table 2. We also executed 1,000 simulations for every case to obtain sufficiently accurate statistical pseudolite position calibration errors. Figure 11 shows results for each case. We can find that Case F, which uses intuitive six points set, is better than Case A, which uses optimal four points set. This shows that the number of calibration points is more important than optimization of calibration points set. In other words, we have to use many calibration points to reduce calibration errors even if computation may be slower. So increasing calibration points is much preferable to optimising them because pseudolite position calibration is a one-time process and optimization is a much more complex process. However, we should consider the optimization results if we increase calibration points and if we want to use a small number of calibration points.

## CONCLUSIONS

This paper proposed a pseudolite position calibration procedure, which uses carrier-phase measurements collected at calibration points, for an indoor navigation system. This procedure is a type of loop, which consists of two subparts. One is to optimize a calibration points set for the estimated pseudolite constellation, and the other is to calculate pseudolite positions using

double-differenced carrier-phase measurements. To optimize calibration points set, we used linearized error covariance of pseudolite positions as a performance index. We used ICDGPS to calculate pseudolite positions. To estimate the effectiveness of our procedure in pseudolite position calibration, we performed simulations for various cases. First, we calculated optimal four and six calibration points set for our indoor navigation pseudolite constellation. We calculated the trace of optimal four calibration points set to analyze the influence of the reference station receiver's antenna position. As expected, the optimal calibration points set moved according to the reference station receiver's antenna position and they could not be obtained easily by intuition, while it is possible for symmetric case. This means that optimization of calibration points set is more powerful when the reference station receiver's antenna is nonsymmetrically located. Using the optimal calibration points set, we performed simulations to estimate how helpful our procedure can be. We compared the pseudolite position calibration errors using optimal calibration points set with those using an intuitive calibration points set. We defined the intuitive calibration points set as a regular polygon, whose radius is the average distance from the origin of the optimal calibration points set. Simulation results showed that optimal calibration points set is better than an intuitive calibration points set, and a six calibration points set is better than a four calibration points set, even in the intuitive case. This means that the number of calibration points is more important than optimization of calibration points set. However, we should consider the optimization results when we arrange calibration points and if we want to use a smaller number of calibration points. We would like to think that this paper provides some standards for arranging calibration points for pseudolite position calibration. In addition, the simulation results showed that all the pseudolite positions could be calibrated with two or three centimeters using only four or six calibration points. In addition, we can calculate the exact phase centre of pseudolite antenna as we use carrier-phase measurements. Therefore, we could say that this paper provided a practical and accurate method to calibrate pseudolite positions for indoor navigation system.

## REFERENCES

1. H.S. Cobb, GPS pseudolites: Theory, design, and applications, Ph.D. Dissertation of AA, Stanford University, (September 1997).
2. G. Elkaim, M. O'Connor, T. Bell and B.W. Parkinson, System identification and robust control of a farm vehicle using CDGPS, In *Proceedings of ION-GPS 1997*, Kansas City, MO, pp. 1415–1426, (1997).
3. J.M. Stone and J. Powell, $4^{th}$ *International Symposium on Space Navigation Technology and Applications*, Brisbane, Australia, (1999).
4. K.R. Zimmerman, Experiments in the use of the global positioning system for space vehicle rendezvous, Ph.D. Dissertation of EE, Stanford University, (December 1996).
5. E.H. Teague, Flexible structure estimation and control using the global positioning system, Ph.D. Dissertation of AA, Stanford University, (May 1997).
6. E. Olsen, C. Park and J. How, 3D formation flight using differential carrier-phase GPS sensors, In *Proceedings of ION-GPS 1998*, Nashville, TN, pp. 1947–1956, (1998).
7. C. Kee, H. Jun, D. Yun, B. Kim, Y. Kim, B.W. Parkinson, T. Lenganstein and S. Pullen, Development of indoor navigation system using pseudolites, In *Proceedings of ION-GPS 2000*, Salt Lake City, UT, pp. 1038–1046, (2000).
8. C.A. Balanis, *Antenna Theory: Analysis and Design*, Second Edition, pp. 505–512, John Wiley & Sons, New York, (1997).
9. J.N. Little and L. Shure, *MATLAB Optimization Tool Box*, Mathworks, (1992).